Physica Medica 131 (2025) 104937

Contents lists available at ScienceDirect

Physica Medica

journal homepage: www.elsevier.com/locate/ejmp

Cone beam CT (CBCT) in radiotherapy: Assessment of doses using a pragmatic setup in an international setting

Mario Djukelic [a,b,*], Colin John Martin [c,d], Abdullah Abuhaimed [e,b], Tomas Kron [f,g,d], Sebastien Gros [h,d], Tim Wood [i,d], Piotr Pankowski [j,b], Ngie Min Ung [k,d], Jenia Vassileva [l,d], María Cristina Plazas [b,m,n], Snezana Vostinic [o,b], Anja Lazovic [o,b], Ana Cravo Sá [p,q,b], Isabelle Nilsson [r,s,b], Marianna Koutrouli [t,b], Lavanya Murugan [u,b], Hein Fourie [v,b], Aliaksandr Miadzvetski [w,b], Buthaina Al Ameri [x,b], Mirta Dumancic [y,z,b], Anson Ho-Yin Cheung [aa,b], Zakiya Al Rahbi [ab,b], Yiannis Roussakis [ac,b], Hossam Ragab Shaaban [ad,b], Runcheng Liang [ae,b], Nada Tomic [y,z], Daniel Eduardo Salazar Correa [af,ag], Duncan Butler [a,ah], William Small Jr. [h,d]

[a] *Department of Medical Technology and Physics, Sir Charles Gairdner Hospital, Nedlands WA 6009, Australia*
[b] *Mentorship programme, International Commission on Radiological Protection, 280 Slater Street, Ottawa, Ontario K1P 5S9, Canada*
[c] *Department of Clinical Physics and Bio-Engineering, University of Glasgow, Gartnavel Royal Hospital, Glasgow G12 0XH, UK*
[d] *Task Group 116 member, International Commission on Radiological Protection, 280 Slater Street, Ottawa, Ontario K1P 5S9, Canada*
[e] *King Abdulaziz City for Science and Technology (KACST), P.O. Box: 6086, Riyadh, Saudi Arabia*
[f] *Department of Physical Sciences, Peter MacCallum Cancer Centre, 305 Grattan Street, Melbourne VIC 3000, Australia*
[g] *Centre for Medical Radiation Physics, University of Wollongong, Australia*
[h] *Loyola University Chicago, Stritch School of Medicine, Department of Radiation Oncology, Cardinal Bernardin Cancer Center, Maywood, IL 60153, USA*
[i] *Medical Physics Service, Queen's Centre, Castle Hill Hospital, Hull University Teaching Hospitals NHS Trust, Castle Road, Hull HU16 5JQ, UK*
[j] *Department of Nuclear Physics and Radiation Safety, Faculty of Physics and Applied Informatics University of Lodz, Pomorska 149/153, 90-236 Lodz, Poland*
[k] *Clinical Oncology Unit, Faculty of Medicine, Universiti Malaya, 50603 Kuala Lumpur, Malaysia*
[l] *Radiation Protection of Patients Unit, International Atomic Energy Agency, Vienna International Centre, PO Box 100, 1400 Vienna, Austria*
[m] *Physics Department, Sciences Faculty, Universidad Nacional de Colombia, Bogotá, Colombia*
[n] *Cancer Institute "Carlos Ardila Lülle", Santa Fe Foundation, Bogota, Colombia*
[o] *National Cancer Research Centre, University of Belgrade, Belgrade, Serbia*
[p] *Centro de Ciências e Tecnologias Nucleares, Instituto Superior Técnico, Universidade de Lisboa, Campus Tecnológico e Nuclear, Estrada Nacional 10, Km 139.7, 2695-066 Bobadela LRS, Portugal*
[q] *Center for Translational Health and Medical Biotechnology Research (TBIO)/Health Research Network (RISE-Health), School of Health, Polytechnic University of Porto, Rua Dr. António Bernardino de Almeida, 400, 4200-072 Porto, Portugal*
[r] *Department of Hematology, Skane University Hospital, Lund, Sweden*
[s] *Medical Radiation Physics, Lund University Hospital, Lund, Sweden*
[t] *Medical Physics, Newcastle upon Tyne Hospitals NHS Foundation Trust, Newcastle, UK*
[u] *Department of Radiation Oncology & Medical Physics, Rajiv Gandhi Government General Hospital and Madras Medical College, Chennai, India*
[v] *Netcare Ltd, 76 Maude Street, Corner West Street, Sandton, South Africa*
[w] *N.N. Alexandrov National Cancer Centre of Belarus, Liasny, Belarus*
[x] *Federal Authority for Nuclear Regulation (FANR), Abu Dhabi, United Arab Emirates*
[y] *Medical Physics Unit, Department of Oncology, Faculty of Medicine, McGill University, Montreal, Quebec, Canada*
[z] *Lady Davis Institute for Medical Research, Jewish General Hospital, Montreal, Quebec, Canada*
[aa] *Hong Kong Baptist Hospital, 222 Waterloo Road, Hong Kong*

* Corresponding author.
E-mail addresses: mario.djukelic@health.wa.gov.au (M. Djukelic), colinmartin1948@gmail.com (C.J. Martin), aabuhaimed@kacst.edu.sa (A. Abuhaimed), Tomas.Kron@petermac.org (T. Kron), SEGROS@lumc.edu (S. Gros), tim.wood3@nhs.net (T. Wood), piotr.pankowski@uni.lodz.pl (P. Pankowski), nmung@ummc.edu.my (N.M. Ung), j.n.vassileva@gmail.com (J. Vassileva), mcplazasd@unal.edu.co (M.C. Plazas), svostinic@gmail.com (S. Vostinic), anjalazovic@ymail.com (A. Lazovic), anacravosa@ctn.tecnico.ulisboa.pt (A.C. Sá), Isabelle.M.Nilsson@skane.se (I. Nilsson), maria.koutrouli@nhs.net (M. Koutrouli), lavanive04@gmail.com (L. Murugan), Hein.Fourie@netcare.co.za (H. Fourie), aliaksandr.miadzvetski@gmail.com (A. Miadzvetski), buthaina.alameri@fanr.gov.ae (B.A. Ameri), mirta.dumancic@mail.mcgill.ca (M. Dumancic), ansonhycheung@hkbh.org.hk (A.H.-Y. Cheung), z.alra7bi@gmail.com (Z.A. Rahbi), Yiannis.Roussakis@goc.com.cy (Y. Roussakis), Hossam.Ragab1992@outlook.sa (H.R. Shaaban), liangruncheng@gmail.com (R. Liang), ntomic@jgh.mcgill.ca (N. Tomic), dsalazarco@unal.edu.co (D.E. Salazar Correa), Duncan.Butler@arpansa.gov.au (D. Butler), wmsmall@lumc.edu (W. Small).

https://doi.org/10.1016/j.ejmp.2025.104937
Received 1 September 2024; Received in revised form 9 February 2025; Accepted 10 February 2025
Available online 21 February 2025

[ab] Department of Radiation Oncology, National Oncology Centre, Royal Hospital, Muscat, Oman
[ac] Department of Medical Physics, German Oncology Center, European University Cyprus, Limassol, Cyprus
[ad] Warith International Cancer Institute, Al-Horr Road, Karbala, Iraq
[ae] Nuclear and Radiation Frontier Technology Research Center, China Institute for Radiation Protection, Taiyuan, Shanxi, PR China
[af] Hospital Universitario Nacional de Colombia, Cl. 44 #59-75, Teusaquillo, Bogotá, Colombia
[ag] Los Cobos Medical Center, Ak. 9 #131a-40, Usaquén, Bogotá, Colombia
[ah] Australian Radiation Protection and Nuclear Safety Agency, Primary Standards Dosimetry Laboratory, Yallambie, VIC 3085, Australia

ARTICLE INFO

Keywords:
Image-guided radiotherapy
kV cone beam computed tomography
Cone beam dose index
Water equivalent phantom
On-board imager
Dosimetry
Farmer ionisation chamber
Correction factor

ABSTRACT

Introduction: The imaging modality kV CBCT on linear accelerators (linacs) is utilised to verify positioning and anatomy in cancer patients undergoing radiotherapy treatment. There is a need for optimisation of radiological protection in kV CBCT imaging protocols to avoid unnecessarily high exposures to normal tissues surrounding the target.
Methods: A network of ICRP mentees from 23 countries were surveyed for available dosimetry equipment. Standardised measurements on CBCT linac imaging systems were conducted using a cone beam dose index (CBDI) devised as a straightforward measurement for wide beam doses. Measurements were made with (a) 100 mm ionisation chambers or (b) 0.6 cc Farmer ionisation chambers and cylindrical CT PMMA phantoms, and (c) an alternative setup of Farmer chambers and cubical phantoms comprised of slabs of water equivalent material readily available in radiotherapy centres. The measurements were compared with Monte Carlo (MC) simulations.
Results: The survey showed limited availability for the reference setup using 100 mm chambers and CT phantoms. Correction factors were derived to convert normalised CBDI from alternative setups to the reference setup and are on average within 2% of MC simulations.
Conclusion: The slab phantom in combination with a Farmer chamber provides an alternative to quantify CBCT radiation dose indices from linac-based image-guided radiotherapy using materials accessible in most centres worldwide. A method is presented to use correction factors for Varian Truebeam linacs if traditional 100 mm chambers and cylindrical CT phantoms are not available. This will enable most radiotherapy centres across the world to engage in meaningful imaging dose measurement and optimisation.

1. Introduction

Technological advances in external beam radiotherapy (RT) equipment with linear accelerators (linacs) over the last two decades now allow radiation fields to be delivered more conformally to the shapes of individual tumours. Treatment plans are generally based on computed tomography (CT) images acquired on a diagnostic quality CT scanner with the patient in treatment position. Pre-treatment and intra-fraction images of patients are usually acquired and compared to planning CT images prior to treatment delivery to ensure reproducibility of the patient and anatomy positioning in order to achieve a successful treatment outcome. These images are commonly recorded with kV x-ray imaging units attached to the linacs, and these allow the x-ray tube and image receptor to be rotated around the patient to produce cone beam CT (CBCT) scans. Pre-treatment and intra-fraction imaging can be carried out at frequencies ranging from once per course of treatment to more than once per treatment fraction [24]. This Image-Guided Radiation Therapy (IGRT) concept has enabled significant improvements in sparing normal tissue through better localisation of therapeutic beams [12], and has allowed dose escalation to tumours while keeping doses to organs at risk (OARs) below tolerance levels. However, these improvements should be offset against the additional radiation doses to the surrounding organs and tissues from imaging, as these will raise OAR doses as well as risks of second primary cancers in other tissues [9]. Therefore, it is important to optimise the radiological protection of CBCT scans, particularly as they can potentially be repeated at each fraction or acquired multiple times per fraction.

Task Group 116 of the International Commission on Radiological Protection (ICRP) was established in 2018 to prepare guidance on radiological protection in IGRT. Through the ICRP mentorship programme, mentees collaborated with radiation therapy centres worldwide to gather data on imaging practices, revealing kV cone beam computed tomography (CBCT) as the primary modality, but with limited centres recording CBCT imaging dose indices [24]. To optimize radiological protection in imaging, surveys on patient imaging dose indices are crucial [19,20]. The first step in surveying patient dose indices is the choice of a quantity to be measured.

Various techniques for measuring CBCT dose indices have been summarised and challenges such as obtaining full scatter conditions have been discussed [13]. The International Electrotechnical Commission [22] derives a quantity akin to the CT dose index (CTDI) used in CT scanner dosimetry that can be measured with a large phantom and a long ionisation chamber. The International Atomic Energy Agency (IAEA) described a method for making the measurement with standard CT dosimetry equipment [17]. This technique involves measurement of the $CTDI_{100}$ for a narrow reference beam with a 100 mm long ionisation chamber, in a standard cylindrical polymethyl methacrylate (PMMA) CT phantom, 150 mm long and with 320 mm in diameter for the body or 160 mm for the head. A value for the CTDI for the wide beam used for imaging is then derived by multiplying this by a factor equal to the ratio of CT doses measured in free air for the wide cone beam measured with a long 300 mm ionisation chamber and for the reference beam measured with a 100 mm chamber. The measurement with a long 300 mm chamber can be simulated by summing measurements with a 100 mm chamber moved across the beam in 100 mm steps [22,17]. This technique gives a $CTDI_{IEC}$ that equates to the $CTDI_{100}$ used for dosimetry on standard CT scanners that is independent of beam width [26,6–7]. Values can be measured at the centre ($CTDI_c$) and periphery ($CTDI_p$) of cylindrical CT phantoms and combined to give a weighted CTDI ($CTDI_w$) similar to that used for standard CT scans. This is the recommended quantity for display on CBCT systems employed in radiotherapy and the accuracy of the displayed value can be verified using the technique referred to above [17].

Another technique proposed by the American Association of Physicists in Medicine (AAPM) [4–5] and the International Commission on Radiation Units and Measurements (ICRU) [21] aims to derive the dose at the centre of a scan of a phantom to account for scattered radiation, in order to provide a more realistic assessment of the maximum dose to tissues of a patient during a scan. The AAPM/ICRU technique involves measurements of the dose with a Farmer type ionisation chamber at the centre of a cylindrical phantom that is 450 mm [4] or 600 mm long [4–5], sufficient to capture all the scatter radiation [7]. Another study

[27] used a triple phantom configuration aligning three CT head or body phantoms back-to-back to obtain full scatter conditions. These techniques provide dose indices that can be used as standard accurate assessments of dose to a patient. However, the IAEA method involves multiple measurements that take significant time to carry out and the AAPM method requires specialised equipment that is not available in most RT centres [18].

The present study was undertaken with the aim of developing methods through which surveys of patient doses from imaging could be performed. For this purpose, a quantity is needed that is relatively easy to measure and uses dosimetry equipment that is readily available in RT centres. Amer et al. [8] suggested measurement of cone beams with a 100 mm ionisation chamber in a standard 150 mm long PMMA cylindrical phantom, in which the cone beam covers the whole CT phantom, to give a quantity called the cone beam dose index (CBDI). This involves measurement of the dose for a single CBCT scan rotation, but instead of the x-ray beam only irradiating a narrow section within the phantom, the 150 mm long phantom lies entirely within the cone beam. Dose measurements can be made at the centre and periphery of the phantom and combined to derive a weighted value, as for the standard $CTDI_w$. This approach utilises equipment that is more readily available in hospitals and has been applied in clinical practice [30,7,10,32]. The CBDI was adopted as the measurement quantity for use in the surveys, but although RT centres in some countries have access to 100 mm ionisation chambers and phantoms needed for the measurements, it soon became apparent that many of those in low- and middle-income countries and even some high-income ones do not have this equipment at present.

A project was established through the ICRP mentorship programme to investigate the feasibility of carrying out patient CBCT dose index surveys in a range of countries across the world [25]. The first stage of this project involved obtaining information on the availability of ionisation chambers and phantom materials in RT centres. The second stage explored methods to measure quantities related to the CBDI using these materials, followed by practical trials in several RT centres across the world. The measurements and survey information were obtained by the network of TG116 mentees from the ICRP mentorship programme, that is referred to as the TG116 Mentee Network. The TG116 Mentee Network obtained data from the following countries: Australia, Belarus, Brazil, Canada, China, Colombia, Cyprus, Egypt, Greece, Hong Kong, India, Iraq, Italy, Malaysia, Oman, Poland, Portugal, Saudi Arabia, Serbia, South Africa, Spain, Sweden, United Arab Emirates, United Kingdom (UK), and United States of America.

2. Materials and methods

2.1. Survey of equipment availability

The TG116 Mentee Network was extended from eight initial mentees to include participants from 23 countries for the purpose of assessing and testing dosimetry techniques. To collect information on the availability of radiation-measuring instruments and phantoms, an Excel survey form was distributed across the mentee network asking for assessments of the availability of phantoms and instruments in RT centres within their countries. The equipment options included were 100 mm and 0.6 cc Farmer type ionisation chambers, 32 cm and 16 cm cylindrical CT dosimetry phantoms, slabs of water equivalent or tissue equivalent phantom material, and availability of calibration coefficients for kV x-ray beam qualities for the Farmer ionisation chambers. Initial discussions with the mentees revealed that equipment availability varied based on the income and development levels of the participating countries. Therefore, the collected data were categorized according to the Human Development Index (HDI) value, as defined by the United Nations Development Programme [31]. The HDI combines indices of life expectancy and education with per capita income, and values increase with the level of development up to a maximum of 1.0.

2.2. Farmer chamber calibration coefficient

The survey revealed that most radiotherapy centres have Farmer chambers calibrated to absorbed dose to water at Co-60 beam qualities as per IAEA TRS 398 Revision 1 dosimetry protocol [16]. The exception is if a radiotherapy centre offers superficial orthovoltage therapy or has access to diagnostic imaging medical physicists on site. The following Farmer chamber calibration coefficient (FCCC) is applied in measurements obtained with Farmer chamber calibrated to absorbed dose to water at Co-60 beam qualities.

$$FCCC = \frac{N_{k,Q}}{N_{D,w,Co60}} \tag{1}$$

where $N_{k,Q}$ and $N_{D,w,Co60}$ are the calibration coefficients in terms of air kerma and absorbed dose to water at user (Q) and reference (Co-60) beam quality respectively. The Australian primary standards dosimetry laboratory (PSDL) located at the Australian Radiation Protection and Nuclear Safety Agency (ARPANSA) provided $N_{D,w,Co60}$ and $N_{k,Q}$ factors determined from 28 PTW TM30013 Farmer type ionisation chambers (PTW Freiburg GmbH, Germany) at relevant beam qualities expressed in half value layers (HVL) that are typically used in kV CBCT imaging in IGRT. The chambers were measured in Co-60 in water (buildup cap off), in Co-60 in air (buildup cap on) and in air with a medium energy x-ray beam (buildup cap off).

2.3. Comparison of Farmer and 100 mm ionisation chambers in CT phantom

The standard CTDI definition is designed for application to narrow beam widths, which makes its usage unsuitable for the purpose of this study. The $CTDI_c$ and $CTDI_p$ are measured air kerma in the central and peripheral positions of the cylindrical PMMA CT phantom that are normalised based on the beam width and ion chamber length, respectively. A weighted value combining these measurements is determined with the following equation:

$$CTDI_w = \frac{1}{3}CTDI_c + \frac{2}{3}\left(\frac{1}{4}\sum_{i=1}^{4} CTDI_{p_i}\right) \tag{2}$$

For this project, similar equipment was used for measuring the CBDI with a wide cone beam. Depending on equipment availability, the TG116 Mentee Network carried out CBDI measurements on the cylindrical body or head CT phantoms using both a 0.6 cc Farmer and a 100 mm ionisation chamber. Participants were required to position the phantom at the isocentre of the CBCT rotation axis and measure air kerma in the centre and four peripheral positions in the CT phantom in a standardised way similar to the traditional CTDI method [2], but using a wide beam that covered the entire phantom to determine a normalised $CBDI_w$ [8] analogously to Equation (2):

$$Normalised\,CBDI_w = \frac{1}{total\,mAs} \times \left[\frac{1}{3}CBDI_c + \frac{2}{3}\left(\frac{1}{4}\sum_{i=1}^{4} CBDI_{p_i}\right)\right] \tag{3}$$

Where $CBDI_c$ and $CBDI_{p_i}$ are the measured air kerma in the centre and the peripheral positions of the CT phantom, and total mAs is the exposure used in the given kV CBCT imaging protocol. Note that the cone beam covers the entire length of the 100 mm chamber, so no normalisation based on the beam width and chamber length is required, unlike in the CTDI method mentioned above. The CBDI methodology described by Amer et al. stipulates additional scatter material to be placed inferior and superior to the cylindrical CT phantom to achieve scatter equilibrium in the centre of the phantom. However, this was not performed in this study to maintain a simplified setup.

A standardised Excel spreadsheet and specific work instructions were distributed within the TG116 Mentee Network. Local technique parameters of the head, pelvis, and thorax kV CBCT imaging protocols as

well as the linac model and RT centre information were recorded. The measurements were performed with the appropriately sized CT phantom (head or body) depending on the choice of kV CBCT imaging protocol, and available ionisation chamber (Farmer, 100 mm, or both). Per definition, measurements performed with the 100 mm ion chamber are referred to $CBDI_w$. Measurements carried out with the 0.6 cc ion chamber are referred to $CBDI_{w,f}$.

The final goal is to measure $CBDI_w$ for the total exposure given by the imaging protocol without normalising to mAs, i.e. cumulative $CBDI_w$. This will allow the comparison of imaging dose values between different centres to evaluate relative patient dose levels. However, for this initial investigation, the $CBDI_w$ measurements were normalised with respect to exposure to compare different measurement systems. The differences in normalised $CBDI_w$ determined with the Farmer chamber and the 100 mm chamber were analysed and compared with Monte Carlo (MC) simulations [7]. By considering $CBDI_w$ measured with a 100 mm chamber as the reference method, ion chamber ratios (IR) between measurements of the two chambers were calculated as:

$$IR = \frac{CBDI_w}{CBDI_{w,f}} \tag{4}$$

The ion chamber ratio can be used as a correction factor if 100 mm chambers are not available.

2.4. Slab phantom method to measure $CBDI_{w,f}$(slab)

In addition to the CBDI measurements in CT phantoms, the TG116 Mentee Network performed measurements using an alternative setup. This setup used a 0.6 cc Farmer ionisation chamber and a 30 x 30 x 30 cm^3 cubical phantom comprising slabs of water equivalent or tissue equivalent material typically used and widely available in RT centres (Fig. 1). This approach was adopted because the survey revealed that many RT centres did not have access to cylindrical PMMA phantoms. Based on basic geometrical calculations, the equivalent cylindrical diameter averaged over a 360° rotation is approximately 33.7 cm, which is similar to the 32 cm CT body phantom. Some of the water or tissue equivalent slabs contain holes designed to fit the dimensions of a Farmer ionisation chamber. These dose measurement slabs can be positioned appropriately to measure doses at the centre and at four peripheral positions around the circumference (Fig. 1). The measurements were performed in a standardised way similar to the traditional CTDI method [2] and the CBDI method [8]. The normalised measured results, referred to as $CBDI_{w,f}$(slab), were determined using Equation (3). Specific work instructions and standardised Excel spreadsheets were provided to the Mentee Network.

The main difference from the CBDI measurements conducted with the cylindrical CT phantom is that the water equivalent phantoms were from various manufacturers and had several different compositions, depending on availability at the local RT centre. The majority of slab phantoms were comprised of PTW RW3 (PTW Freiburg GmbH, Germany) followed by PMMA. A few RT centres from the TG116 Mentee Network provided the following phantoms: Plastic Water – The Original (Sun Nuclear Corporation, USA, previously CIRS, USA); Plastic Water – The Original (75 %) + Virtual Water (25 %) (Standard Imaging, USA); Gammex Solid Water (Sun Nuclear Corporation, USA); Gammex Solid Water (21 cm thick) + PMMA (9 cm thick); Standard Imaging Solid Water HE (Standard Imaging, USA); WT1 Solid Water (Phoenix Dosimetry Ltd, UK).

2.5. Monte Carlo simulations of CBDI and slab phantom

A MC model of the imaging system of Varian Truebeam was used to calculate the various CBDI ($CBDI_w$, $CBDI_{w,f}$ and $CBDI_{w,f}$(slab)) for the body and head protocols. The model was tested and validated in previous studies [6,7]. The x-ray beam from the imaging system was simulated with 10^9 particles for each protocol using the EGSnrc-based code (BEAMnrc) [28,23]. The generated particles were saved in files known as phase space at 50 cm from the source, which were transferred to another EGSnrc-based code(egs_chamber) to be used as kV source of the imaging system [33]. The CT body and head phantoms were simulated, and centres of the phantoms were placed 50 cm from the corresponding phase space, which means the isocentre was set to be 100 cm from X-ray source. Two chambers, a 100 mm ionisation chamber (Radcal 10X6-3CT) and a Farmer type ionisation chamber (PTW TM30013) were modelled based on geometric information obtained from the manufacturers. The chambers were used to calculate $CBDI_w$ and $CBDI_{w,f}$, respectively, whereas $CBDI_{w,f}$(slab) values were only calculated with the farmer chamber. The x-ray sources were rotated around the phantoms over 360 and 200 degrees for the body and head protocols, respectively. Doses were computed for each protocol at central and peripheral positions, from which the various CBDI were assessed. Similarly, the chemical compositions of the 30 x 30 x 30 cm^3 water or tissue equivalent phantoms were obtained from the manufacturer, upon which the slab phantom was designed with egs_chamber code. The PMMA phantom was also created with the same size, and centres of the phantoms were placed at the isocentre 100 cm from the

Fig. 1. Positioning of water or tissue equivalent slab phantom (here: PTW RW3) and Farmer type ionisation chamber at the isocentre of the kV CBCT On-Board Imager on a Varian Truebeam linac. Left: Farmer chamber in the central position to measure $CBDI_{c,f}$(slab). Right: Farmer chamber in the right peripheral position to measure one of the four $CBDI_{p,f}$(slab) values.

source. Only the Farmer chamber was used for this setup, and doses were calculated at the centre and periphery of the solid phantoms in a manner similar to that used for the CT measurements.

The simulations were used to determine phantom ratios (PR) that are expressed in the following equations:

$$PR = \frac{CBDI_w}{CBDI_{w,f}(slab)} \quad (5)$$

$$PR_f = \frac{CBDI_{w,f}}{CBDI_{w,f}(slab)} \quad (6)$$

These phantom ratios can be used as correction factors to determine $CBDI_w$ if 100 mm ionisation chambers and CT phantoms are not available.

The MC conditions ought to match with the measurement conditions to appropriately compare measured and simulated IR and PR. The MC conditions are referred to as the "Truebeam Group". IR or PR measurements are added to the Truebeam Group if a radiotherapy centre was able to meet the MC equipment conditions described in this section.

3. Results

3.1. Survey of equipment availability

Data on equipment availability are provided in Fig. 2, where countries are grouped according to HDI value in the bands > 0.9 (higher income), 0.8 to 0.9, and < 0.8 (lower income). The stacked columns report on the proportion of countries within a HDI band that had equipment availability in all RT centres (100 % – blue), in more than half of RT centres (>50 % – orange) and less than half of RT centres (<50 % – grey) in their country.

Across all HDI bands, only 26 % of all surveyed countries had 100 mm ionisation chambers and CT phantoms available in all RT centres, with less than half of the high-income countries and no low-income countries having access in all radiotherapy centres. In comparison, across all HDI bands, 78 % of all surveyed countries had 0.6 cc Farmer chambers and slab phantoms in all RT centres and the remaining 22 % in over half of the RT centres in their country.

Based on this data it was decided that where cylindrical CT phantoms and 100 mm ionisation chambers were available these would be used for the method of choice for dosimetry. Measurements with Farmer chambers in cylindrical phantoms would be explored as an alternative where no 100 mm chamber was available. For RT centres without cylindrical phantoms the use of a 30 × 30 × 30 cm^3 slab phantom with a Farmer chamber would be investigated as a possible alternative technique for body CT dosimetry.

3.2. Farmer chamber calibration coefficient

Table 1 shows $N_{k,Q}/N_{D,w,Co60}$ ratios measured at the PSDL at ARPANSA. The ratios were averaged across 28 PTW TM30013 Farmer ionisation chambers. The beam qualities are typically measured on a kV CBCT system of a Varian Truebeam linac and are in the range of HVL measurements performed by the Mentee Network. SD is the standard deviation. The average ratio across the six beam qualities is 0.89 with an uncertainty (k = 1) of 0.01. As the ratio is constant across the beam qualities, the FCCC for this study determined with Equation (1) is defined at FCCC = 0.89.

3.3. Comparison of Farmer and 100 mm ionisation chamber in CT phantom

Table 2 summarises the normalised $CBDI_w$ measured with CT head and body phantom and 100 mm ionisation chamber grouped by linac models, phantom size, tube voltages, filtration and collimation. Varian TrueBeam, VitalBeam and Edge models were grouped together as well as

Table 1
$N_{k,Q}/N_{D,w,Co60}$ ratios averaged across 28 PTW TM30013 Farmer ionisation chambers measured at various beam qualities at the Australian primary standards dosimetry laboratory at the Australian Radiation Protection and Nuclear Safety Agency. The beam qualities are typically measured in a kV CBCT imaging system of a Varian Truebeam linac. SD is the standard deviation.

Beam quality Q		Mean of 28 PTW TM30013 Farmer chamber measurements
kV	HVL (mmAl)	$N_{k,Q}/N_{D,w,Co60}$ (SD)
140	7.195	0.891 (0.006)
150	7.582	0.891 (0.005)
100	6.614	0.892 (0.006)
120	7.588	0.892 (0.005)
140	8.436	0.892 (0.005)
150	8.832	0.892 (0.005)

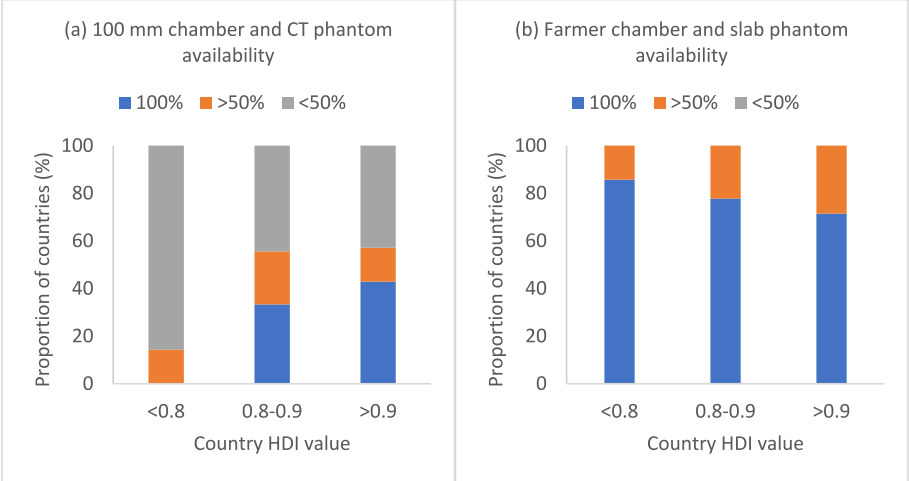

Fig. 2. Bar charts showing the availability of dosimetry equipment within RT centres in terms of proportion of centres with both the ionisation chambers and phantoms in 23 countries taking part in the study, grouped according to human development index (HDI) values. The equipment involved is (a) 100 mm ionisation chambers and cylindrical PMMA CT phantoms and (b) 0.6 cc Farmer ionisation chambers and water equivalent slab phantoms according to HDI value in the bands > 0.9 (higher income), 0.8 to 0.9, and < 0.8 (lower income). The stacked columns report on the proportion of countries within a HDI band that had equipment availability in all RT centres (100 % – blue), in more than half of the RT centres (>50 % – orange) and less than half of RT centres (<50 % – grey) in their country.

Table 2
Normalised $CBDI_w$ measured with CT head and body phantom and 100 mm ionisation chamber grouped by linac models, phantom size, kV, filtration and collimation. The normalised $CBDI_w$ per 100 mAs was compared to a published reference from a UK survey of 63 RT centres [32]. N is the number of linac measurements and IQR is the inter quartile range.

Manufacturer and Model	CT Phantom	Filter	Collimator	kV	Normalised $CBDI_w$ (mGy/100 mAs)			
					This study		UK study	
					N	Median (IQR)	N	Median (IQR)
Varian TrueBeam / VitalBeam / Edge	Head	Full	–	100	38	2.4 (0.2)	29	2.3 (0.3)
	Body	Half	–	125	67	1.7 (0.1)	43	1.8 (0.1)
	Body	Half	–	140	20	2.3 (0.1)	10	2.3 (0.2)
	Body	Full	–	125	10	1.8 (0.1)	7	1.9 (0.1)
Varian Clinac / Trilogy	Head	Full	–	100	17	3.4 (0.3)	11	3.5 (0.4)
	Body	Half	–	125	8	2.8 (0.6)	9	3.0 (0.1)
	Body	Half	–	110	4	2.4 (0.3)	7	2.3 (0.3)
Elekta XVI	Head	F0	S20	120	5	3.6 (0.5)	15	3.5 (0.2)
	Body	F1	M20	120	5	2.1 (0.2)	19	2.0 (0.4)
	Body	F1	L20	120	4	1.7 (0.2)	12	1.5 (0.2)
Varian Halcyon	Head	–	–	100	6	3.0 (0.2)	–	–
	Body	–	–	125	12	2.1 (0.5)	–	–

Varian Clinac and Trilogy models. Except for Varian Halcyon models, the normalised $CBDI_w$ per 100 mAs was compared to a UK survey that obtained measurements from 63 RT centres across the country [32].

Fig. 3 and Table 3 summarise the comparison of Farmer and 100 mm ionisation chamber measurements in CT phantom. Fig. 3 compares $CBDI_w$ and $CBDI_{w,f}$ measured in cylindrical CT head and body phantoms for 100 kV half arc head and 125 kV full arc body imaging protocols. The ion chamber ratios were calculated with Equation (4) such that paired $CBDI_w$ and $CBDI_{w,f}$ were both measured in a linac under the same imaging conditions. IR are presented in box plots for all linac and Farmer chamber models (Head/Body all), for the Truebeam Group uncorrected (Head/Body Truebeam) and corrected for Farmer chambers calibrated

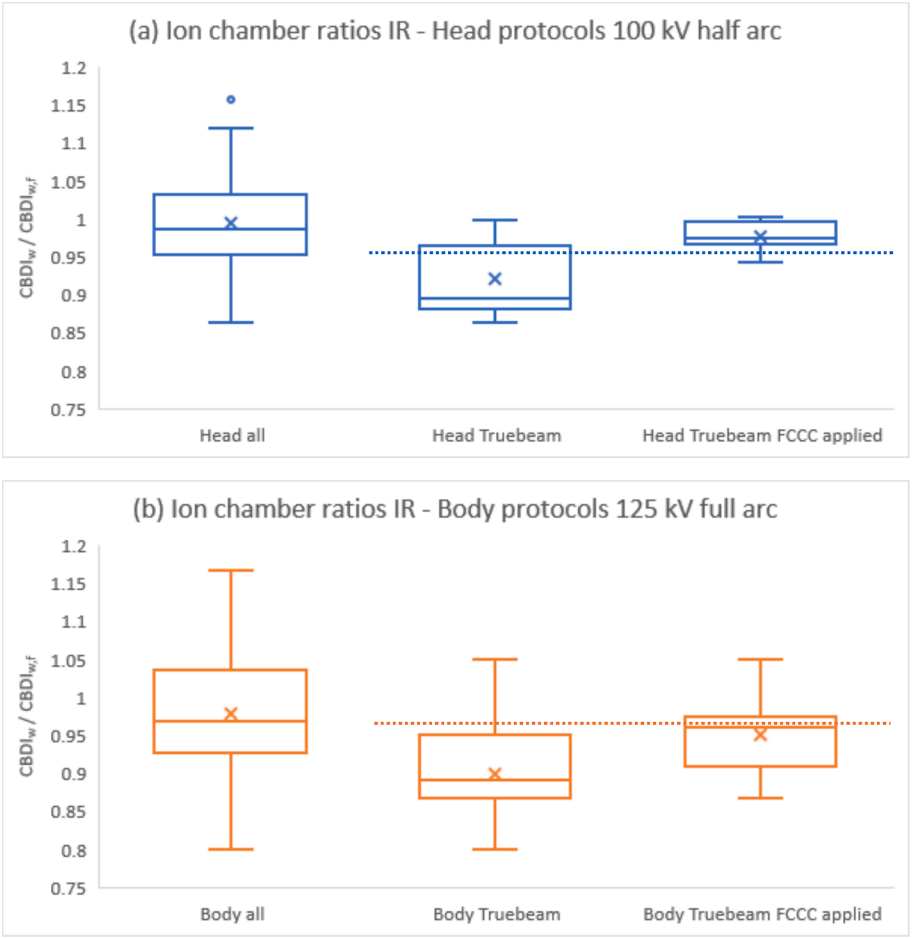

Fig. 3. Comparison of normalised $CBDI_w$ and $CBDI_{w,f}$ measured in cylindrical CT phantoms for CBCT imaging protocols representing (a) the head for a 100 kV half arc protocol and (b) the body for a 125 kV full arc (thorax and pelvis) protocol. Ion chamber ratios IR were calculated with Equation (4) where each $CBDI_w$ and $CBDI_{w,f}$ pair were measured in a linac under the same imaging conditions. IR presented in box plots for all linac and Farmer chamber models (Head/Body all), for the Truebeam Group uncorrected (Head/Body Truebeam) and corrected with the Farmer chamber calibration coefficient (FCCC) (Head/Body Truebeam FCCC applied). The 'x' and the inner line are presenting the mean and median respectively. The circles are outliers. The box shows the interquartile range and the whiskers show the range. Dashed line shows Truebeam MC simulation values.

Table 3
Ratios of measurements $CBDI_w/CBDI_{w,f}$ and $CBDI_w/CBDI_{w,f}(slab)$ made with 100 mm ionisation chamber in cylindrical CT phantoms to similar measurements made with a Farmer chamber in a cylindrical phantom (IR, Equation (4)) and in slab phantoms made from PTW RW3 and PMMA phantoms (PR, Equation (5)). Results are shown for all linacs combined and the Truebeam Group uncorrected and with the Farmer chamber calibration coefficient (FCCC) applied. The results are compared with Monte Carlo simulations. N is the number of paired linac measurements. SD is the standard deviation.

	Ion chamber ratios				Phantom ratios			
	Head		Body		PTW RW3		PMMA	
	Mean (SD)	N	Mean (SD)	N	Mean (SD)	N	Mean (SD)	N
All	0.99 (0.07)	45	0.98 (0.09)	76	0.97 (0.12)	36	0.85 (0.09)	15
Truebeam	0.92 (0.05)	11	0.90 (0.06)	22	0.88 (0.07)	9	0.82 (0.05)	9
Truebeam FCCC applied	0.97 (0.03)	11	0.95 (0.04)	22	0.90 (0.06)	9	0.88 (0.04)	9
Monte Carlo*	0.96 (0.01)	–	0.97 (0.01)	–	0.90 (0.01)	–	0.89 (0.01)	–

*For cone beam widths greater than 100 mm [7].

in absorbed dose to water (Head/Body Truebeam FCCC applied). Within the Truebeam Group, the FCCC (Equation (1)) was applied on measurements that used Farmer chambers calibrated to absorbed dose to water at Co-60 beam qualities. The 'x' and the inner line present the mean and median respectively. The box shows the interquartile range (IQR) and the whiskers show the range. The circles are outliers. Dashed line shows Truebeam MC simulation values. A substantial portion, amounting to 38%, of CT phantom measurements were excluded for the direct comparisons between 100 mm and Farmer chamber as these RT centres only had access to a Farmer type ionisation chamber.

3.4. Slab phantom method to measure $CBDI_{w,f}(slab)$

Similarly, Fig. 4 and Table 3 summarise the comparison of slab phantom and CT phantom measurements. Fig. 4 compares determined $CBDI_w$ and $CBDI_{w,f}(slab)$ measured in PTW RW3 and PMMA slab phantoms for kV CBCT 125 kV full arc body imaging protocols. Note, that Elekta results are for 120 kV. The phantom ratios (PRs) were calculated with Equation (5) such that paired $CBDI_w$ and $CBDI_{w,f}(slab)$ were measured in a linac under the same imaging conditions. PR are presented in box plots for all linac and Farmer chamber models (PTW/PMMA all), for the Truebeam Group uncorrected (PTW/PMMA Truebeam) and corrected for Farmer chambers calibrated in absorbed dose to water (PTW/PMMA Truebeam FCCC applied). Within the Truebeam

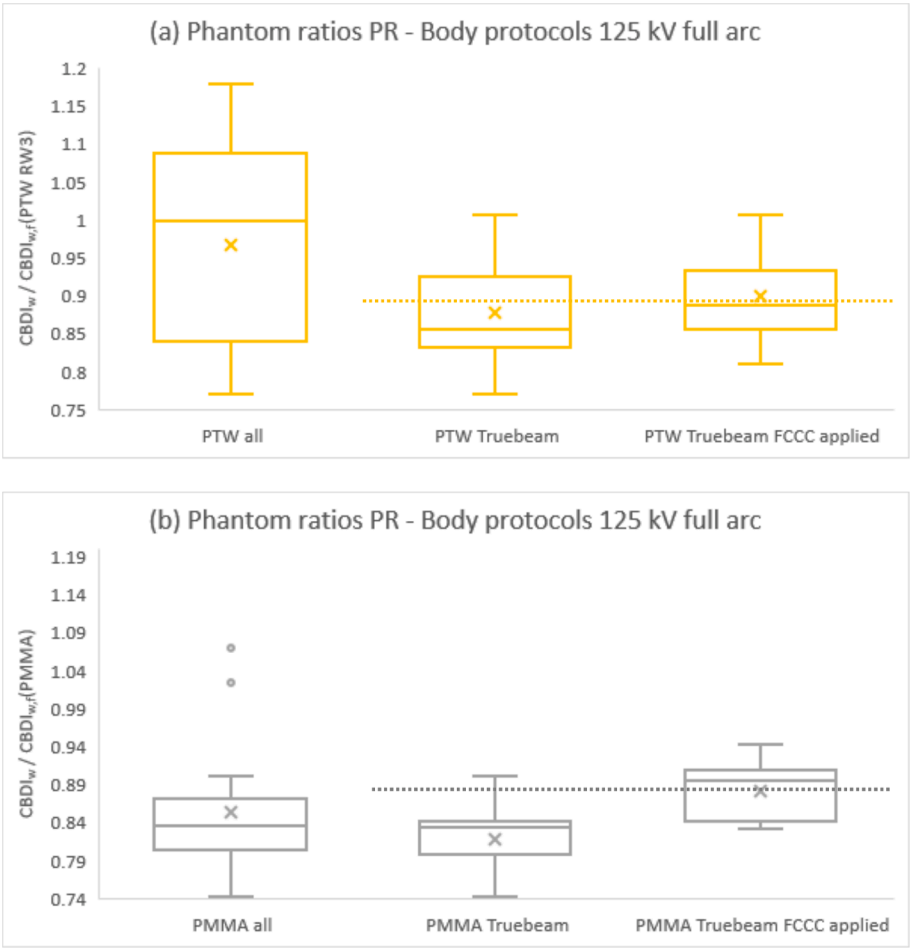

Fig. 4. Comparison of normalised $CBDI_w$ and $CBDI_{w,f}(slab)$ for CBCT body 125 kV full arc body imaging protocols measured in slab phantoms made from (a) PTW RW3 and (b) PMMA. Phantom ratios PR were calculated with Equation (5) where each $CBDI_w$ and $CBDI_{w,f}(slab)$ pair were measured in a linac under the same imaging conditions. PR presented in box plots for all linac and Farmer chamber models (PTW/PMMA all), for the Truebeam Group uncorrected (PTW/PMMA Truebeam) and corrected with the Farmer chamber calibration coefficient (FCCC) (PTW/PMMA Truebeam FCCC applied). The 'x' and the inner line present the mean and median respectively. The box shows the interquartile range and the whiskers show the range. The circles are outliers. Dashed line shows Truebeam MC simulation values.

Group, the FCCC (Equation (1)) was applied to measurements that used Farmer chambers calibrated to absorbed dose to water at Co-60 beam qualities.

Fig. 5 shows PR and PR_f results determined with Equation (5) and (6) respectively. These present the phantom ratios of other linac models for completion. Ratios of measurements for the cylindrical CT phantom and the slab phantom with Farmer chambers (Equation (6)) for Elekta linacs yielded a ratio of 0.91 ± 0.07 (14 data sets). This compared to a ratio of 0.90 ± 0.05 for measurements with 100 mm chambers in the cylindrical phantom and Farmer chambers in the slab phantoms (10 data sets) for Elekta (Equation (5)).

Table 4 shows basic statistical results for average peripheral $CBDI_p$ to central $CBDI_c$ ratios for CT phantoms as well as PTW RW3 and PMMA slab phantoms. Included were measurements from 125 kV full arc body imaging protocols.

3.5. Recommended correction factors for Truebeam Group

Table 5 summarises the correction factors to convert measurements to $CBDI_w$ for the Truebeam Group if 100 mm ionisation chambers and cylindrical CT phantom are not available. It presents the factors that can be applied to correct to the reference method, i.e. 100 mm ionisation chamber and cylindrical head/body CT phantom. The user can select the correction factor depending on the available equipment and the available Farmer chamber calibration used for the measurements.

For the air kerma calibrations, the mean and standard deviation from the physical measurements were used as correction factors and uncertainties (k = 1) respectively (Table 3). For the absorbed dose to water calibrations, these means were multiplied with the FCCC from Equation (1) to use as a correction factor. The uncertainties were calculated as a combined uncertainty of the physical measurements' standard deviation (Table 3) and the uncertainty of the FCCC data from ARPANSA PSDL (Table 1).

4. Discussion

4.1. Survey of equipment availability

This study investigated alternative methods for measuring kV CBCT dose indices in IGRT based on measurement data and surveys on equipment availability obtained from an international cohort. The results from the RT equipment survey (Fig. 2) suggest that RT centres and hospitals in most countries have limited access to cylindrical CT phantoms and 100 mm ionisation chambers typically used to determine

Table 4
Basic statistical results for average peripheral ($CBDI_p$) to central ($CBDI_c$) ratios for cylindrical CT, and PTW RW3 and PMMA slab phantom, for kV CBCT body 125 kV full arc body imaging protocols. N is the number of linac measurements, SD is the standard deviation and IQR is the interquartile range.

Peripheral CBDI to Central CBDI ratios			
Phantom	**Physical measurements**		
	N	**Mean (SD)**	**IQR**
$CBDI_p/CBDI_c$	130	1.43 (0.16)	0.14
$CBDI_{p,f}/CBDI_{c,f}$	82	1.45 (0.18)	0.09
$CBDI_{p,f}(PTWRW3)/CBDI_{c,f}(PTWRW3)$	43	1.40 (0.12)	0.13
$CBDI_{p,f}(PMMA)/CBDI_{c,f}(PMMA)$	10	1.40 (0.03)	0.04

tomographic imaging dose indices. This is especially true for low-income countries with HDI levels less than 0.8. It indicates the need to explore an alternative dosimetry method in order to enable surveys of patient imaging dose indices to be carried out in a broader range of countries. Use of water or tissue equivalent slab phantoms with Farmer chambers that are available in the majority of RT centres could be an option if appropriate correction factors are applied.

4.2. Comparison of Farmer and 100 mm ionisation chamber in CT phantom

The normalised $CBDI_w$ for a variety of linac models, phantom size, tube voltages, filtration and collimation were compared with data obtained from a UK survey encompassing measurements from 63 RT centres across the country [32]. Median differences in normalised $CBDI_w$ ranged from 0.1 mGy/100 mAs to 0.2 mGy/100 mAs (Table 2), supporting the validity and constancy of the measurements of this study. Additionally, this study provides normalised $CBDI_w$ for Varian Halcyon for 100 kV and 125 kV imaging protocols. These normalised $CBDI_w$ can be used to calculate cumulative $CBDI_w$ by multiplying with the protocol's total exposure (mAs) if physical measurements are not possible due to limited equipment availability.

The ion chamber ratio IR in normalised $CBDI_w$ between 100 mm and Farmer ionisation chamber measurements in CT phantoms for the Truebeam Group FCCC applied were on average 0.97 and 0.95 for the head and body protocols respectively (Table 3). The expected ratios from a previous study [7], that are based on MC simulations (dashed lines in Fig. 3) for beam widths greater than 100 mm (active chamber length) are slightly different at 0.96 and 0.97. The boxplots showed that the range of IR is higher when including all linac models (Fig. 3 "Head all", "Body all") as expected due to a variety of model-based filtration

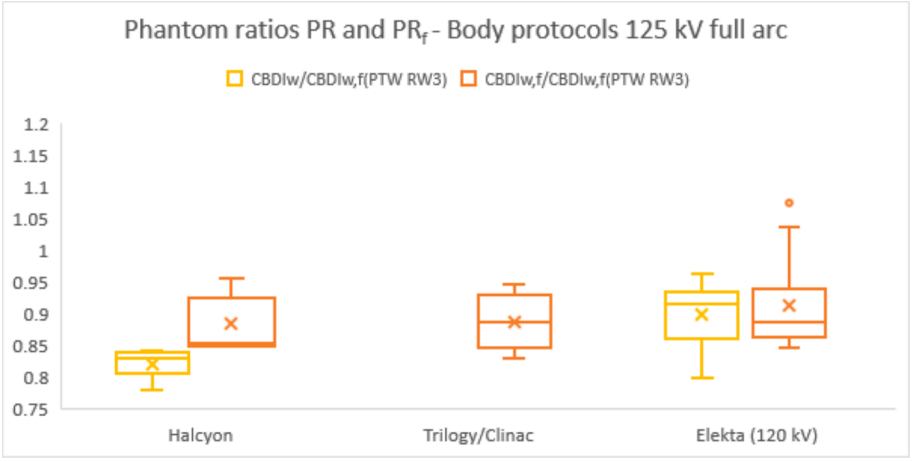

Fig. 5. Comparison of normalised $CBDI_w$ and $CBDI_{w,f}$(slab) for body 125 kV (or 120 kV) full arc body imaging protocols measured in slab phantoms made from PTW RW3. PR and PR_f were calculated with Equation (5) and (6) respectively and are shown for other linac models. The 'x' and the inner line present the mean and median respectively. The box shows the interquartile range and the whiskers show the range. The circles are outliers.

Table 5
Correction factors to convert to $CBDI_w$ for the Truebeam Group.

Correction factor	Correcting to	Available equipment	Available Farmer chamber calibration	Correction factor (uncertainty k = 1)
$CBDI_w/CBDI_{w,f}$(Head Protocols 100 kV half arc)	CT head phantom and 100 mm ionisation chamber	CT head phantom and Farmer ionisation chamber (PTW TM30013)	Air kerma – 100 kV beam quality	0.97 (0.03)
			Absorbed dose to water – Co-60 beam quality	0.86 (0.03)
$CBDI_w/CBDI_{w,f}$(Body Protocols 125 kV full arc)		CT body phantom and Farmer ionisation chamber (PTW TM30013)	Air kerma – 125 kV beam quality	0.95 (0.04)
			Absorbed dose to water – Co-60 beam quality	0.84 (0.04)
$CBDI_w/CBDI_{w,f}(PTWRW3)$(Body Protocols 125 kV full arc)	CT body phantom and 100 mm ionisation chamber	PTW RW3 slab phantom and Farmer ionisation chamber (PTW TM30013)	Air kerma – 125 kV beam quality	0.90 (0.06)
			Absorbed dose to water – Co-60 beam quality	0.80 (0.06)
$CBDI_w/CBDI_{w,f}(PMMA)$(Body Protocols 125 kV full arc)		PMMA slab phantom and Farmer ionisation chamber (PTW TM30013)	Air kerma – 125 kV beam quality	0.88 (0.04)
			Absorbed dose to water – Co-60 beam quality	0.79 (0.04)

and geometries. The boxplots also showed that the IR range decreases for the Truebeam Group when applying the FCCC that accounts for Farmer chambers calibrated to absorbed dose to water at Co-60 beam qualities.

The small differences between measured and simulated IR suggest that the Farmer chamber can be used as an alternative if a 100 mm type chamber is not available in a RT centre. The Farmer chambers measure the dose over a shorter distance in the middle of the phantom. The contribution from scattered x-rays will gradually decline away from the middle and the smaller Farmer chamber will almost entirely lie within the dose peak and so register a higher dose reading, relative to the 100 mm chamber.

38% of CT phantom measurements were excluded for the direct comparisons between 100 mm and Farmer chamber as these RT centres only had access to a Farmer type ionisation chamber. This emphasises the necessity of deriving correction factors that convert Farmer measurements in a CT phantom to the reference method (Table 5).

4.3. Slab phantom method to measure $CBDI_{w,f}(slab)$

Fig. 4 and Table 3 summarise the comparison of simulated MC and measured phantom ratios. The results focussed on PTW RW3 and PMMA as these were the most commonly used slab phantoms. The measured phantom ratios PR using PTW RW3 and PMMA for the Truebeam Group FCCC applied were on average 0.90 and 0.88 compared to the simulated PR of 0.90 and 0.89 respectively. The difference between measured and simulated PR is visualised by the dashed lines in Fig. 4. The demonstrated small differences between measured and simulated PR show that the PTW RW3 and PMMA slab phantoms combined with a Farmer type ionisation chamber for the Truebeam Group can be used as an alternative if a 100 mm chamber and cylindrical CT phantoms are not available in a RT centre. Notably, Fig. 5 showed that other linac models such as Varian Halcyon, Trilogy, Clinac, and Elekta at 120 kV differ on average by 0–8 % from the Truebeam Group PTW RW3 simulations.

Comparing phantom ratios (PR) and ion chamber ratios (IR), it is evident that $CBDI_{w,f}(slab)$ is relatively higher than $CBDI_{w,f}$. The CT phantom is standardised in terms of dimensions and composition. In contrast, water equivalent materials typically used in RT centres have a variety of compositions depending on the manufacturer [29] and are developed for the purpose of dosimetry in the MeV photon range as opposed to keV. In terms of composition, the PTW RW3 contains titanium, which has a higher probability of photoelectric absorption in the keV range given the high atomic number. In terms of phantom dimensions, Table 4 showed that the ratio between measured peripheral and central doses is different for the cubically shaped slab phantoms and the cylindrically shaped CT phantom. For example, with the slab phantom, the position of the chamber for peripheral dose measurements is further from the x-ray tube focus than in the cylindrical phantom, while the average thickness of attenuating material through which x-rays pass before reaching the central chamber will be slightly greater. In addition, the slab phantom extends further along the z-axis of the CBCT, so there will be a larger contribution from scatter from the ends of the phantom. The differences between PMMA slab and CT phantom is due to different geometry rather than material as the latter is essentially a cylinder made of PMMA.

4.4. Farmer chamber calibration coefficient

The boxplots in Fig. 3 and Fig. 4 showed that the ion chamber ratios IR and phantom ratios PR ranges decrease for the Truebeam Group when applying the FCCC accounting for Farmer chambers calibrated to absorbed dose to water at Co-60 beam qualities. This underlines the need and the strength of the FCCC. The calibration methods used for the 100 mm and Farmer chamber are based on varying beam qualities and inherent uncertainties in calibration values. The 100 mm ionisation chamber is typically air kerma calibrated for photons in the keV range used in diagnostic imaging. Farmer chambers can be calibrated in a similar manner for low energy keV photons [3,34]. However, for radiotherapy in the MeV photon range, ionisation chambers are calibrated in terms of absorbed dose to water with a Co-60 beam [1,16].

Some RT centres offer superficial orthovoltage therapy, which requires the use of Farmer chambers calibrated in the keV photon range. While these chambers are indeed calibrated in the keV range, the calibration process for orthovoltage therapy involves different added filtration compared to calibration of chambers used in diagnostic imaging [3]. A limited number of publications provide calibration coefficient ratios for reference chambers calibrated in term of absorbed dose to water in Co-60 and in terms of air kerma [11,14,15]. A computed average of the ratios $N_{k,Co60}/N_{D,w,Co60}$ from these publications provides a factor of 0.91 for PTW TM30013 Farmer ionisation chambers. This is comparable with the FCCC of 0.89 derived from the ARPANSA PSDL data. The ARPANSA data also showed that the $N_{k,Q}/N_{D,w,Co60}$ ratios for PTW TM30013 are constant across the relevant beam qualities Q meaning there is no need for additional diagnostic keV beam quality corrections such as k_{Q,Q_0} as defined in IAEA TRS 398 Revision 1 [16].

The general ion chamber ratio IR and phantom ratio PR ranges in the boxplots shown in Fig. 3 and Fig. 4 can also be attributed to the inherent uncertainties of ionisation chamber measurements. The manufacturers of the 100 mm ionisation chambers used in this study quoted measurement uncertainties of 4–5 %. Additionally, the national dosimetry laboratories of the Farmer ionisation chamber used in this study quoted measurement uncertainties of 0.86–2 %.

4.5. Recommended correction factors

Table 5 shows a set of recommended correction factors that allows simple conversion to normalised $CBDI_w$ for the Truebeam Group. Correction factors are provided for following alternative setups:

- CT head phantom and Farmer ionisation chamber
- CT body phantom and Farmer ionisation chamber
- PTW RW3 slab phantom and Farmer ionisation chamber
- PMMA slab phantom and Farmer ionisation chamber

Correction factors also consider the available Farmer chamber calibration:

- Air kerma at 100 kV beam quality – $N_{k,100kV}$
- Air kerma at 125 kV beam quality – $N_{k,125kV}$
- Absorbed dose to water at Co-60 beam quality –$N_{D,w,Co60}$

These correction factors were derived from physical measurements from an international sample and data obtained from the Australian PSDL at ARPANSA. The presented comparisons showed small differences between measured and simulated ion chamber ratios IR and phantom ratios PR (Fig. 3, Fig. 4 and Table 3) indicating that the recommended correction factors can be used when utilising alternative measurement setups.

4.6. Outlook

The study evaluated $CBDI_w$, $CBDI_{w,f}$ and $CBDI_{w,f}$(slab) normalised to the total tube current exposure. The aim of the work was to develop methods through which values for the doses for individual imaging procedures can be compared. This would enable identifying RT centres using protocols that deliver higher dose levels and require optimisation of kV CBCT imaging protocols. A future study will investigate the use of cumulative CBDI as a metric to compare kV CBCT imaging doses between RT centres at both national and international levels. As cumulative CBDI is a metric without normalisation of exposure, it can be used for imaging protocol optimisation, dose awareness, and the determination of dose reference levels. RT centres would have the ability to identify and review high dose imaging protocols by initiating a formal optimisation process in a multi-disciplinary team comprised of medical physicists, radiation oncologists and therapy radiographers / radiation technologists. Well optimised imaging protocols have the potential to reduce the radiation burden to the patients' OARs without a significant compromise of image quality.

At this stage the MC simulations were only performed on the Truebeam Group due to limited supercomputing resources. However, the presented results showed that the measured and simulated IR and PR are a good match for the Truebeam Group. This indicates the high quality of the MC model which can be used in future studies to validate correction factors on other linac models, slab phantom vendors and Farmer chamber models.

The alternative slab phantom has dimensions of 30 x 30 x 30 cm^3, which is not appropriate for head imaging protocols. This limitation will be investigated in a future study considering alternative phantom options that have a similar equivalent cylindrical diameter as the 16 cm CT head phantom.

5. Conclusion

The study compares the weighted cone beam dose index normalised to the exposure determined with a cylindrical CT phantom and an alternative water or tissue equivalent slab phantom setup from an international sample of RT centres. The results suggest that the slab phantom provides an alternative setup to assess kV CBCT doses that can be used in imaging protocol optimisation for RT centres that do not have standard CT measuring chambers and cylindrical phantoms at the present time. It also provides a simple and pragmatic check system for constancy of dose delivered over time. Moreover, the results suggest that a 0.6 cc Farmer type ionisation chamber can be used with the cylindrical CT phantom as an alternative if 100 mm type ionisation chambers are not available. Accessibility to equipment is an important factor to consider as the international survey showed that 100 mm and cylindrical CT phantoms are not available in many RT centres. To overcome this issue, this study presents a set of recommended correction factors, which can be used to give a standard dose quantity, that can be evaluated through available alternative equipment. This will facilitate comparisons of imaging doses between RT centres. The method using CT phantoms should be used, where they are available, and the slab phantom option, at other centres. This would enable measurements to be made that relate to the cumulative dose with mAs values used for clinical measurements, and hence surveys of CBCT doses to be performed to compare dose levels for imaging at different centres. This allows RT centres to identify and review imaging protocols with high cumulative doses triggering an optimisation process to ultimately lower the radiation burden to the patients' OARs. Methods such as that proposed, using tools that are available locally will hopefully allow a move to more inclusive development of standards for imaging in RT.

Declaration of competing interest

The authors declare that they have no known competing financial interests or personal relationships that could have appeared to influence the work reported in this paper.

Acknowledgments

The authors would like to thank the supercomputing lab at King Abdullah University of Science and Technology (KAUST) for their permission of performing all Monte Carlo simulations on the supercomputer (SHAHEEN). The authors would also like to thank the International Commission on Radiological Protection (ICRP) for establishing the mentorship programme enabling Task Group 116 affiliated mentees to contribute to this international study. Moreover, the authors would like to express their sincere gratitude to all radiotherapy centres who enabled the mentees to perform measurements on their linacs and equipment. Finally, the authors would like to extend their gratitude to the Australian primary standards dosimetry laboratory at the Australian

Radiation Protection and Nuclear Safety Agency (ARPANSA) for the expert advice on Farmer chamber calibration methods and providing important data used for the presented Farmer chamber calibration coefficient.

References

[1] AAPM. Almond, P.R., et al. "AAPM's TG-51 protocol for clinical reference dosimetry of high-energy photon and electron beams.". Med Phys, 1999;26: 1847–70.
[2] AAPM. The measurement, reporting, and management of radiation dose in CT. AAPM Report 96. American Association of Physicists in Medicine; 2008.
[3] AAPM, 2001. Ma, C-M., et al. "AAPM protocol for 40–300 kV x-ray beam dosimetry in radiotherapy and radiobiology." Medical physics 28.6 (2001): 868-893.
[4] AAPM, 2010 Comprehensive methodology for the evaluation of radiation dose in x-ray computed tomography. Report of AAPM Task Group 111: The Future of CT Dosimetry. AAPM, MD.
[5] AAPM, 2020 Task Group No. 200—The Design and Use of the ICRU/AAPM CT Radiation Dosimetry Phantom: An Implementation of AAPM Report 111, AAPM Report 200.
[6] Abuhaimed A, Martin C J, Sankaralingam M, et al., 2014 An assessment of the efficiency of methods for measurement of the computed tomography dose index (CTDI) for cone beam (CBCT) dosimetry by Monte Carlo simulation Phys. Med. Biol. 59 6307–26.
[7] Abuhaimed A, Martin CJ, Sankaralingam M, et al. A Monte Carlo investigation of cumulative dose measurements for cone beam computed tomography (CBCT) dosimetry. Phys Med Biol 2015;60(4):1519–42.
[8] Amer A, Marchant T, Sykes J, Czajka J and Moore C 2007 Imaging doses from the Elekta Synergy x-ray cone beam CT system Br. J. Radiol. 80 476–82.
[9] Alaei P, Spezi E (2015) Imaging dose from cone beam computed tomography in radiation therapy. Phys Med 31:647–658. https:// doi. org/ 10. 1016/j. ejmp. 2015. 06. 003.
[10] Buckley JG, Wilkinson D, Malaroda A, et al. Investigation of the radiation dose from cone-beam CT for image-guided radiotherapy: A comparison of methodologies. J Appl Clin Med Phys 2018;19(1):174–83.
[11] Csete I, et al. Report on EUROMET. RI (I)-K1 and EUROMET. RI (I)-K4 (EUROMET project no. 813): Comparison of air kerma and absorbed dose to water measurements of {sup 60} Co radiation beams for radiotherapy. Metrologia 2010; 47.
[12] Dawson LA, Sharpe MB. Image-guided radiotherapy: rationale, benefits, and limitations. Lancet Oncol 2006;7(10):848–58.
[13] de Las Heras Gala H, Torresin A, Dasu A, Rampado O, Delis H, Girón IH, Theodorakou C, Andersson J, Holroyd J, Nilsson M, Edyvean S. Quality control in cone-beam computed tomography (CBCT) EFOMP-ESTRO-IAEA protocol (summary report). Physica Medica. 2017 Jul 1;39:67-72.
[14] Hassan GM, et al. Impact of Beam Quality Q for 137Cs on NK and ND,W for Different Types of Ionization Chambers. Appl Phys Res 2011;3–1.
[15] IAEA, 1996 Czap, L, Matschenko, G, Andreo, P, Intercomparison of ionization chamber calibration factors in the IAEA/WHO network of SSDLs, SSDL Newsletter Issue No. 35, IAEA 1996, https://www.iaea.org/publications/4890/ssdl-newsletter-issue-no-35-july-1996, accessed August 2024.
[16] IAEA, 2024 INTERNATIONAL ATOMIC ENERGY AGENCY, Absorbed Dose Determination in External Beam Radiotherapy, Technical Reports Series No. 398 (Rev. 1), IAEA, Vienna (2024), https://doi.org/10.61092/iaea.ve7q-y94k.
[17] IAEA, 2011 Status of computed tomography dosimetry for wide cone beam scanners. IAEA Human Health Reports 5, IAEA, Vienna.
[18] ICRP. Radiological Protection in Cone Beam Computed Tomography (CBCT). ICRP Publication 129. Ann ICRP 2015;44(21).
[19] ICRP. Diagnostic reference levels in medical imaging. ICRP Publication 135. Ann ICRP 2017;46(1).
[20] ICRP. Optimisation of Radiological Protection in Digital Radiology Techniques for Medical Imaging. ICRP Publication 154. Ann ICRP 2024;53(1).
[21] ICRU. ICRU Report No. 87: Radiation dose and image-quality assessment in computed tomography. J ICRU 2012;12:1–149.
[22] IEC. Amendment 1 to IEC 60601–2–44: 2009 Medical electrical equipment: part 2–44. Particular Requirements for the Basic Safety and Essential Performance of x-Ray Equipment for Computed Tomography Committee Draft (CD) 62B/804/CD. Geneva: International Electrotechnical Commission; 2009.
[23] Kawrakow I, Rogers DWO, Mainegra-Hing E, Tessier F, Townson RW, Walters BRB. EGSnrc toolkit for Monte Carlo simulation of ionizing radiation transport 2000. https://doi.org/10.4224/40001303.
[24] Martin, C.J, Kron, T., Vassileva, J. et al., 2021. An international survey of imaging practices in radiotherapy. Phys. Med. 90, 53-65.
[25] Martin, C.J., Gros, S., Kron, T., et al., 2023. Factors affecting implementation of radiological protection aspects of imaging in radiotherapy. Appl. Sci. 13, 1533.
[26] Platten, D.J., Castellano, I.A., Chapple, C.L., Edyvean, S., Jansen, J.T., Johnson, B. and Lewis, M.A., 2013. Radiation dosimetry for wide-beam CT scanners: recommendations of a working party of the Institute of Physics and Engineering in Medicine Br. J. Radiol. 86, 1027, 20130089.
[27] Rampado O, Giglioli FR, Rossetti V, Fiandra C, Ragona R, Ropolo R. Evaluation of various approaches for assessing dose indicators and patient organ doses resulting from radiotherapy cone-beam CT. Med Phys 2016;43(5):2515–26.
[28] Rogers DWO, Faddegon BA, Ding GX, Ma CM, We J, Mackie TR. BEAM: A Monte Carlo code to simulate radiotherapy treatment units. Med Phys 1995;22:503–24.
[29] Schoenfeld AA, Harder D, Poppe B, Chofor N. Water equivalent phantom materials for 192Ir brachytherapy. Phys Med Biol 2015;60(24):9403.
[30] Sykes, J.R., Lindsay, R., Iball, G., et al., 2013. Dosimetry of CBCT: methods, doses and clinical consequences. In Journal of Physics: Conference Series (Vol. 444, No. 1, p. 012017). IOP Publishing.
[31] UN, 2024. United Nations Development Programme. Human Development Index (HDI). http://hdr.undp.org/en/content/human-development-index-hdi (accessed 16 Feb, 2024).
[32] Wood TJ, Davis A, Earley J, Edyvean S, Findlay U, Lindsay R, et al. IPEM topical report: the first UK survey of cone beam CT dose indices in radiotherapy verification imaging for adult patients. Phys Med Biol 2024.
[33] Wulff J, Zink K, Kawrakow I. Efficiency improvements for ion chamber calculations in high energy photon beams. Med Phys 2008;35:1328–36.
[34] IAEA, 2007 Dosimetry in diagnostic radiology: an international code of practice. IAEA technical report series 457, IAEA, Vienna.